High-frequency longitudinal and transverse dynamics in water

E. Pontecorvo,[1,4] M. Krisch,[2] A. Cunsolo,[3] G. Monaco,[2] A. Mermet,[2] R. Verbeni,[2] F. Sette,[2] and G. Ruocco[1,4]
[1]*Dipartimento di Fisica and INFM, Universitá di Roma "La Sapienza," I-00185, Roma, Italy*
[2]*European Synchrotron Radiation Facility, Boîte Postal 220, F-38043 Grenoble, France*
[3]*Institut Laue-Langevin, BP 156, F-38043 Grenoble, France*
[4]*CRS SOFT, INFM, Universitá di Roma "La Sapienza," I-00185, Roma, Italy*
(Received 24 September 2004; published 11 January 2005)

High-resolution, inelastic x-ray scattering measurements of the dynamic structure factor $S(Q,\omega)$ of liquid water have been performed for wave vectors Q between 4 and 30 nm^{-1} in distinctly different thermodynamic conditions ($T=263-420$ K; at, or close to, ambient pressure and at $P=2$ kbar). In agreement with previous inelastic x-ray and neutron studies, the presence of two inelastic contributions (one dispersing with Q and the other almost nondispersive) is confirmed. The study of their temperature and Q dependence provides strong support for a dynamics of liquid water controlled by the structural relaxation process. A viscoelastic analysis of the Q-dispersing mode, associated with the longitudinal dynamics, reveals that the sound velocity undergoes a complete transition from the adiabatic sound velocity (c_0) (viscous limit) to the infinite-frequency sound velocity (c_∞) (elastic limit). On decreasing Q, as the transition regime is approached from the elastic side, we observe a decrease of the intensity of the second, weakly dispersing feature, which completely disappears when the viscous regime is reached. These findings unambiguously identify the second excitation to be a signature of the transverse dynamics with a longitudinal symmetry component, which becomes visible in $S(Q,\omega)$ as soon as the purely viscous regime is left.

DOI: 10.1103/PhysRevE.71.011501 PACS number(s): 61.20.−p, 61.10.Eq, 78.70.Ck, 63.50.+x

I. INTRODUCTION

Water occupies a prominent role in natural sciences, partly due to its relative abundance and central role for the existence of life on earth, but as well due to its many unusual properties, which—despite intensive research efforts—still defy today a complete understanding [1,2]. It is believed that the peculiar physicochemical behavior of water arises from its local structure which is characterized by an open three-dimensional hydrogen-bond network of water molecules with an almost perfect tetrahedral arrangement and a well-structured second coordination shell. The hydrogen bond is responsible for this highly ordered local structure, and it is therefore clear that the processes of H-bond breaking and formation play a central role in determining the dynamical and thermodynamical properties of liquid water. The lifetime of the H bond is, at ambient conditions, in the picosecond range. Thus, the study of the water dynamics in the terahertz frequency range is of particular interest. Traditionally, this is done by inelastic scattering techniques using neutrons (INS) or x rays (IXS), or by molecular dynamics (MD) studies. More recently, the high-frequency dynamics has been studied experimentally by time-domain spectroscopy [3,4]. The key quantity in most of these studies is the so-called dynamical structure factor $S(Q,\omega)$ ($\hbar Q$ and $\hbar\omega=E$ denote the momentum and energy transfer, respectively), which is the time and space Fourier transform of the atomic density-density pair correlation function [5]. Starting from the pioneering work by Bosi *et al.* [6] and by Teixeira *et al.* [7], several neutron experiments [8–10] and x-ray studies [11–17] have been devoted to the study of the terahertz-frequency dynamics in liquid water.

The most striking result of these INS, IXS, and MD studies is the existence of a particularly large dispersion effect in the sound velocity as a function of frequency. More specifically, at $T=277$ K and ambient pressure, the longitudinal sound velocity increases from its hydrodynamic value $c_0=1500$ to $c_\infty\approx 3200$ m/s. This transition from the hydrodynamic, or zero-frequency, to the infinite-frequency sound regime is directly observed at $Q=2$ nm^{-1} and energy $E=3$ meV. This phenomenon bears strong resemblance to that observed in glass-forming liquids, where the sound velocity dispersion is due to the presence of a structural (or α) relaxation process. If τ_α is the characteristic time of this process, the system has a solidlike elastic behavior for modes with frequency $\Omega(Q)$ satisfying $\Omega(Q)\tau_\alpha \gg 1$ and a viscous one for frequencies such that $\Omega(Q)\tau_\alpha \ll 1$ [here $\Omega(Q)=c(Q)Q$ is the excitation frequency]. A detailed viscoelastic analysis of the dynamic structure factor demonstrated that also in water the transition from low- to high-frequency sound velocity is actually driven by the structural relaxation process [15].

Temperature-dependent IXS studies, in which the density was kept approximately constant to 1 g/cm^3 by changing the pressure, revealed that, as long as τ_α remains in the picosecond region (i.e., in the high-temperature region), it follows an Arrhenius behavior with an activation energy comparable to the hydrogen-bond energy. This result provided a link between the relaxation process and the hydrogen-bond network, and offered an explanation for the microscopic origin of the structural relaxation process in water. On a time scale short with respect to the lifetime of these H-bonded local structures the collective dynamics is very similar to that of the solid state, i.e., ice [12]. In the opposite limit, the local structures have sufficient time to relax, and therefore show a typical liquid behavior. In the intermediate region, for $\Omega(Q)\tau_\alpha\approx 1$, the dynamics of the density fluctuations is strongly coupled with the making and breaking of the hydrogen-bond network.

A second important result, arising from the whole body of INS and IXS studies of liquid water, is the existence of a second excitation in the dynamic structure factor. This second excitation has a (almost) Q-independent energy, and becomes visible only at Q larger than ≈ 4 nm^{-1}. This second feature, observed in the $S(Q,\omega)$ of ambient condition liquid water by INS [6,8–10] and IXS [12,13,16], has been attributed to transverselike dynamics on the basis of a MD study [18] where the comparison between longitudinal and transverse current spectra was performed. The existence of the second feature and its transverse origin can be explained within the same viscoelastic framework that has been successfully used to describe the longitudinal dynamics. Indeed, the transverse dynamics, known to be nonpropagating in liquids, can be actually supported by the liquid structure as soon as the viscous regime is left and the response becomes solidlike. The "transverse" excitation acquires finite intensity in $S(Q,\omega)$—which is only sensitive to the longitudinal molecular motion—because of the lack of order in the structure, leading to a mixing of modes with longitudinal and transverse symmetry [18].

To summarize, the high-frequency dynamics of liquid water seems to be controlled by a relaxation process—whose microscopic dynamics is related to the making and breaking of the hydrogen-bond network—with a characteristic time τ_α. All the modes with frequencies such that $\Omega(Q)\tau_\alpha \ll 1$ see a relaxing local structure (viscous regime), and behave as liquidlike: low sound velocity and no transverselike dynamics identifiable in the longitudinal current. On the contrary the modes with frequency satisfying $\Omega(Q)\tau_\alpha \gg 1$ see a frozen, solidlike, structure and behave as if they were in the glassy phase: elastic response, high sound velocity, and identifiable transverselike dynamics.

A different interpretation for the origin of the two excitations appearing in the $S(Q,\omega)$ of water has recently been proposed by Petrillo *et al.* [9] and by Sacchetti *et al.* [10], who analyzed the INS and IXS data using a solidlike framework: the mode-mode interaction and the symmetry avoided crossing. In this context, the second dispersionless feature is assigned to a local intermolecular vibration, resembling one of the optic modes in ice [19]. Moreover, at variance with Refs. [13,15], where the longitudinal sound velocity dispersion is associated with the interaction of the longitudinal sound waves with a relaxation process, the transition from the hydrodynamic to the fast sound is attributed to the interaction between the sound waves and this opticlike mode. As the symmetry of the two modes is supposed to be the same, the two branches repel each other to avoid crossing, and the high-frequency branch at large Q disperses with a slope larger than that of the low-frequency branch at small Q. This model describes the INS and IXS spectra as well as the viscoelastic model; a definitive conclusion on the correct interpretation of the water dynamics can therefore not be drawn on the basis of a "best fit" procedure. Such a conclusion needs to rely on an experimental basis, such as that brought, for example, from the physical meaning of the parameters entering in the viscoelastic and in the solidlike models, and/or from their dependence on the thermodynamic state.

In this paper we present additional IXS data which significantly extend the thermodynamic region investigated in previous IXS and INS experiments. Moreover, thanks to the increased performance of the IXS instrument, data with better statistical quality could be recorded, allowing an even more reliable extraction of the relevant parameters. The previous IXS study by Monaco *et al.* [15] was focused on the low-Q region (mainly below 7 nm^{-1}) where the second excitation does not give a significant contribution, and a consistent viscoelastic analysis of the whole spectrum could be performed. The present work covers a much larger Q range (from 4 to 30 nm^{-1}) and thermodynamic region by a choice of pressure and temperature such that the relaxation time τ_α changes by more than a decade. At variance with the previous works, this allows us to follow the evolution of the second weakly dispersing feature not only as a function of momentum transfer, but also all the way from the viscous to the elastic limit. The extended thermodynamic and Q regions and the improved statistics allow us to provide overwhelming evidence in favor of (i) a "viscous"—rather than solidlike—origin of the transition from "normal" to "fast" sound in liquid water and (ii) the transverse origin of the low-frequency weakly dispersing feature appearing in the $S(Q,\omega)$. The paper is organized as follows. In Sec. II we present the experimental setup and the information pertinent to the sample cell, the theoretical formalism utilized in the data analysis, and the experimental results. Section III provides the data analysis and the discussion, while Sec. IV draws the conclusions.

II. EXPERIMENT

A. Experimental setup

The experiment was carried out at the Inelastic X-ray Scattering Beamline II (ID28) at the European Synchrotron Radiation Facility in Grenoble, France. The x rays from an undulator source are monochromatized by a cryogenically cooled silicon (111) double-crystal monochromator and a high-energy resolution backscattering monochromator, operating at the silicon (11 11 11) reflection order. The backscattered photons of energy 21.747 keV impinge on a gold-coated toroidal mirror, which provides a focal spot at the sample position of 270 (horizontal) and 80 (vertical) μm^2 full width at half maximum. The incident flux on the sample is 5×10^9 photon/s. The scattered photons are energy analyzed by a Rowland circle five-crystal spectrometer, operating at the same reflection order as the monochromator. The energy-analyzed photons are detected by a Peltier-cooled silicon diode detector which has an intrinsic energy resolution of 400 eV [20]. The dark counts due to electronic and environmental noise amounts to about 0.003 counts/s. The momentum transfer $Q=2k_i\sin(\theta_s/2)$, where k_i is the incident photon wave vector and θ_s is the scattering angle, is selected by rotating the spectrometer around a vertical axis passing through the scattering sample in the horizontal plane. Since there are five independent analyzer systems, spectra at five different momentum transfers can be recorded simultaneously. Their separation amounts to approximately 3 nm^{-1} for the Si (11 11 11) reflection. The energy scans are performed by varying the monochromator temperature while the analyzer temperature is kept fixed. Conversion from the tem-

TABLE I. Thermodynamic conditions of temperature T and pressure P at which the IXS spectra were recorded. The uncertainty of T is ±1 K and that of P is ±1%. Columns 3–5 report the three corresponding thermodynamic quantities used in the data analysis, namely, the mass density ρ, the adiabatic sound velocity c_0, and the shear viscosity η. Their values were obtained from the water equation of state [21]. The freezing point of water at $P = 2$ kbar is 251 K.

T (K)	P (bar)	ρ (g/cm^3)	c_0 (m/s)	η (cP)
263	2000	1.084	1825	2.09
282	2000	1.078	1820	1.32
296	2000	1.073	1840	0.96
321	2000	1.072	1875	0.62
359	2000	1.041	1880	0.38
419	95	0.926	1500	0.19

perature scale to the energy scale is accomplished by the following relation: $\Delta E/E = \alpha \Delta T$, where $\alpha = 2.58 \times 10^{-6}$ is the linear thermal expansion coefficient of silicon at room temperature. The validity of this conversion has been checked by comparing the measured diamond dispersion curve for longitudinal acoustic and optical phonons with well-established inelastic neutron scattering results. The overall experimental resolution is experimentally determined by measuring the scattering from a disordered sample of Plexiglass at a Q transfer of 10 nm^{-1}, corresponding to the first maximum in the static structure factor $S(Q)$, and at $T = 10$ K in order to maximize the elastic contribution to the scattering.

Distilled and deionized water was loaded into a specially designed stainless steel cell, made out of INCONEL-751, which can be pressurized by a hand pump up to 5 kbar and heated up to 700 K. The x-ray beam passes through two 1-mm-thick diamond single-crystal windows with a 2.3 mm aperture. The distance between the two windows, i.e., the sample length along the x-ray beam, was 10 mm. The cell geometry allowed us to cover the relevant momentum transfer regime up to 30 nm^{-1} with a sample length comparable to the x-ray photoabsorption length ($\mu \approx 0.1$ mm^{-1} at $E = 21$ keV). The high-pressure cell was kept in vacuum in order to minimize both temperature gradients and air scattering. The pressure was monitored with a calibrated gauge whose precision is about 1%. The temperature was determined by a Cr-Al thermocouple in direct contact with the main body of the cell with an accuracy of ±1 K. Table I reports the thermodynamic conditions of the experiment as well as the respective shear viscosity (η) and the adiabatic speed of sound (c_0) values.

B. Theoretical formalism and fitting procedure

The theoretical framework used to interpret the experimental spectra is based on the generalized Langevin equation (memory function approach), more specifically on the generalized hydrodynamic description. In this framework the formal structure of the "classical" hydrodynamic regime is retained, but the thermodynamic derivatives and transport coefficients are replaced by functions which can vary in both space (or wave number) and time (or frequency) [22,23]. In recent years, this approach has been successfully applied to the interpretation of the high-frequency dynamics of different systems, including water, and spanning from noble gases [24] to liquid metals [25], as well as from supercooled liquids [26] to glasses [27]. The basic equations are discussed in detail in Ref. [15]; here, we only stress the key points and the details relevant to the present data analysis.

The longitudinal dynamics is described by a Langevin equation for the density-density correlation function $F(Q,t)$:

$$\frac{\partial^2 F(Q,t)}{\partial t^2} + \omega_0^2(Q) F(Q,t) + \int_0^t dt' m_Q(t-t') \frac{\partial F(Q,t')}{\partial t'} = 0; \tag{1}$$

and, consequently, the expression for the $S(Q,\omega)$ [normalized to $S(Q)$], the time Fourier transform of $F(Q,t)$, reads

$$\frac{S(Q,\omega)}{S(Q)} = \frac{1}{\pi} \frac{\omega_0^2 \tilde{m}_Q'(\omega)}{[\omega_0^2 - \omega^2 - \omega \tilde{m}_Q''(\omega)]^2 + [\omega \tilde{m}_Q'(\omega)]^2} \tag{2}$$

where $\tilde{m}_Q'(\omega)$ and $\tilde{m}_Q''(\omega)$ are the real and imaginary parts of the Fourier transform of the memory function $m_Q(t)$. Its generalized form can be written as

$$m_Q(t) = \omega_0^2(Q)[\gamma(Q) - 1] e^{-D_T(Q)Q^2 t} + K_L(Q,t), \tag{3}$$

where $\omega_0^2 = k_B T Q^2/[MS(Q)]$ is the (squared) frequency of the sound wave excitation in the hydrodynamic regime, $\gamma(Q)$ and $D_T(Q)$ are the Q-dependent generalizations of $\gamma = C_p/C_v$ (the constant pressure to constant volume specific heat ratio) and $D_T = \kappa/(\rho C_v)$, κ is the thermal conductivity, $S(Q)$ is the static structure factor, M is the molecule mass, and k_B is the Boltzmann constant. The second contribution to the memory function, $K_L(Q,t)$, a quantity directly related to the longitudinal kinematic viscosity [22,23], is here chosen as

$$K_L(Q,t) = 2\Gamma_\mu(Q)\delta(t) + \Delta^2(Q) e^{-t/\tau_\alpha(Q)}, \tag{4}$$

where $2\Gamma_\mu(Q)\delta(t)$ represents a fast (microscopic or μ) decaying contribution to $K_L(Q,t)$ and the exponential term accounts for the structural (α) relaxation process. τ_α is the Q-dependent time which characterizes the long time tail of $K_L(Q,t)$, and $\Delta^2(Q)$ is the structural relaxation strength which is related to $c_\infty(Q)$ and $c_0(Q)$—the Q-dependent generalizations of the usual infinite frequency and adiabatic sound speeds [28] via $\Delta^2 = (c_\infty - c_0)Q^2$. In summary, the resulting expression for the memory function becomes

$$m_Q(t) = \omega_0^2(Q)(\gamma(Q) - 1) e^{-D_T(Q)Q^2 t} + 2\Gamma_\mu(Q)\delta(t) + \Delta^2(Q) e^{-t/\tau_\alpha(Q)}.$$

It is worth pointing out that the time dependence of the structural relaxation process contribution to the memory function is assumed here to be Debye-like (no stretching is present). This is in apparent contrast to recent findings [4,29] where the existence of a non-negligible stretching ($\beta \sim 0.6$) in the correlation function of supercooled water was observed.

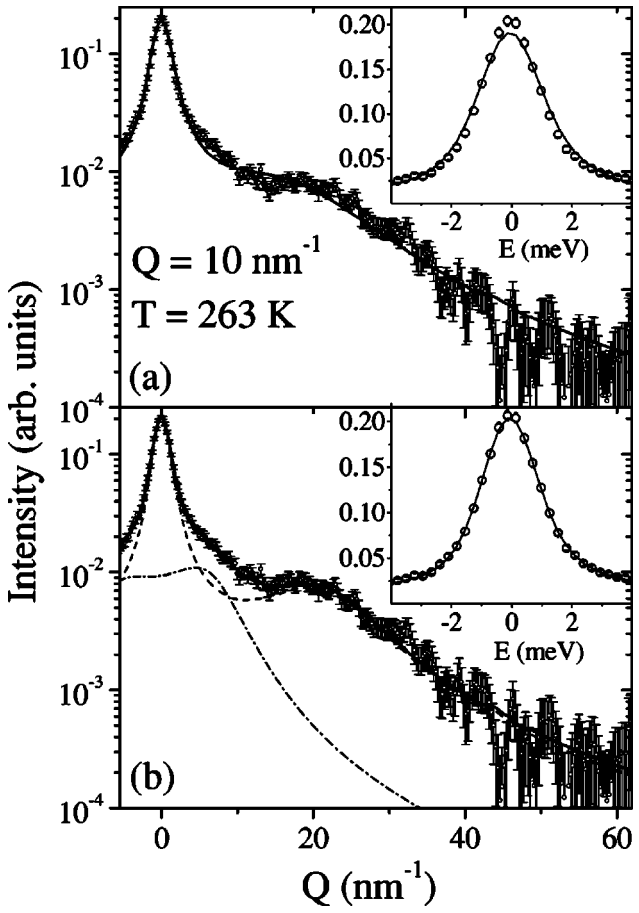

FIG. 1. IXS spectrum at $Q=10\ \mathrm{nm}^{-1}$, $T=263$ K, and $P=2$ kbar. The experimental data and their error bars are shown together with the best fits utilizing the model function described in the text with and without the second inelastic contribution. (a) One viscoelastic contribution. (b) One viscoelastic contribution and one damped-harmonic-oscillator mode. The inset shows the central peak region.

However, as also pointed out in [29], the existence of stretching is hardly detectable in the temperature region investigated here. As a matter of fact, we did not find any significant statistical improvement in introducing an additional fitting parameter (β). We therefore used a simplified version of the memory function and fixed β to 1.

The viscoelastic analysis of the water IXS spectra previously performed [15] was confined to Q values not exceeding $Q=7\ \mathrm{nm}^{-1}$, a region in which the second excitation discussed in the Introduction is not visible. Consequently, the applied theoretical formalism yielded excellent agreement between the model function and the experimental data. In the present case, the inclusion of a second excitation is mandatory as is evident, for example, by inspection of Fig. 1, which reports the IXS spectrum recorded at $T=263$ K, $P=2$ kbar, and $Q=10\ \mathrm{nm}^{-1}$. In this figure, panel (a) shows the best fit to the data with only one excitation (viscoelastic model) according to Eq. (2). Both the inelastic and the central parts of the spectra are not well reproduced, and it is obvious that a second excitation has to be added. This has been done for the fit presented in panel (b) where the second excitation is accounted for by a damped-harmonic-oscillator (DHO) function [30] *added* to the viscoelastic $S(Q,\omega)$, resulting in a significantly better fit. It is important to stress that this is a purely empirical approach to introduce the mixing phenomenon of longitudinal and transverse dynamics. A correct theoretical description should provide a memory function, directly reproducing a double-excitation line shape, which naturally would involve a much larger set of variables. In particular, such a formalism should be extended to the regime of broken ergodicity, when the frequency range is much higher than the structural relaxation time ($\omega\tau_\alpha>1$). In this range the symmetry arguments that decouple the transverse (T) from the longitudinal (L) variables in the generalized Langevin equation must be abandoned and a coupling L-T mechanism must be taken into account. Work along these lines is currently in progress. Within the present context, the choice of a DHO line shape to describe the transverse dynamics is used empirically to provide information on the intensity and the frequency of the second excitation. In summary, the model function used to represent the spectra is composed of the following pieces.

(1) A viscoelastic model function, proportional to Eq. (2), to account for the central peak and the longitudinal dynamics:

$$s^{(L)}(Q,\omega)=\frac{A_L}{\pi}\frac{\omega_0^2\tilde{m}'_Q(\omega)}{[\omega_0^2-\omega^2-\omega\tilde{m}''_Q(\omega)]^2+[\omega\tilde{m}'_Q(\omega)]^2}.$$

We have neglected the contribution due to thermal relaxation, which amounts to setting $\gamma(Q)=1$, an approximation which turns out to be very good in the high-Q region.

(2) A DHO line shape for the second excitation:

$$s^{(T)}(Q,\omega)=\frac{A_T}{\pi}\frac{\Omega_T^2\Gamma_T}{(\Omega_T^2-\omega^2)^2+(\omega\Gamma_T)^2},$$

where Ω_T is the maximum of the "transverselike" contribution to the longitudinal current spectrum [the dynamic structure factor multiplied by ω^2/Q^2, i.e., of $\omega^2 s^{(T)}(Q,\omega)$] and Γ_T is the width of the inelastic transverse peaks.

This model function for the dynamic structure factor is symmetric, and, in order to account for the quantized character of the energy transfers at the microscopic level, has to be weighted with a function that (i) satisfies the detailed balance and (ii) becomes unity in the classical limit ($\hbar\omega/k_BT\ll1$). Among the possible choices, the weighting factor usually utilized is

$$w(\omega,T)=\frac{\hbar\omega}{k_BT}[n(\omega,T)+1]=\frac{\hbar\omega}{k_BT}[1-\exp(-\hbar\omega/k_BT)]^{-1}.$$

Finally, the theoretical model has to be convoluted with the experimental resolution function $R(\omega)$, to give a fitting function of the form

$$I(Q,\omega) = \{R(\omega)\} \otimes \left(\frac{\hbar\omega}{k_B T}[n(\omega,T)+1] \times [s^{(L)}(Q,\omega) + s^{(T)}(Q,\omega)] \right) + B. \quad (5)$$

Here B is an additional term which accounts for the electronic and environmental background of the detectors. As a result, the data are fitted with nine free parameters: (i) the background B; the transverse (ii) "intensity" A_T, (iii) position Ω_T, and (iv) width Γ_T; (v) the longitudinal intensity A_L; the three parameters of the longitudinal memory function, namely, the structural relaxation (vi) time τ_α and (vii) strength Δ and the area of the microscopic relaxation Γ_μ; and, finally, (viii) the static structure factor $S(Q)$ entering in the term ω_0. All these parameters are, in principle, T and Q dependent.

As a matter of fact, Γ_μ, which represents the topological microscopic disorder contribution to the acoustic attenuation, is known to have a negligible temperature dependence. Therefore we have fixed its value to the one obtained at the lowest temperature. We checked that leaving this parameter free does not change significatively the values of the other parameters. Moreover, we observe that, for the highest-temperature spectra, leaving the energy position and width of the transverse contribution as free parameters in the fit results in a meaningless overdamping of the DHO function to the extent that it cannot be distinguished from the purely relaxational elastic contribution already accounted for by the viscoelastic model (the intensity of this contribution vanishes at high T, thus implying that Ω_T and Γ_T become irrelevant). In order to circumvent this, and guided by the observation of Sokolov *et al.* [38], the position and width of the second excitation was unambiguously determined in an unconstrained fit for the lowest-temperature IXS spectra, and kept fixed at higher temperatures. Therefore, at all temperatures but the lowest, there are six free fitting parameters.

C. Experimental results

IXS spectra were recorded at the different temperatures and pressures as indicated in Table I, spanning the momentum transfer, Q, region from 4 to 16 nm^{-1} with an approximate constant spacing of 3 nm^{-1}. For the lowest (263 K) and highest (419 K) temperatures, the Q range was extended to 30 nm^{-1}. The spectra extend up to 60 meV on both sides of the elastic line, with an integration time of 100 s per spectrum. For each setting three spectra were collected, and subsequently summed in order to achieve the high statistical accuracy required for the data analysis. Typical total counts range between 1500 (at 4 nm^{-1}), 2500 (at 9.93 nm^{-1}), and 3500 (at 12.91 nm^{-1}). To account for the slow drift of the photon flux impinging on the sample, the collected data were normalized to the intensity of the incident beam. A typical IXS spectrum is shown on a logarithmic scale in Fig 1. The experimental data with their error bars are shown together with the best fits (full lines) using both the model function discussed before (bottom panel) and the same function with $A_T=0$ (top panel). For clarity, only the elastic and the Stokes part of the spectrum is shown. The insets provide a zoom of the elastic line region on a linear scale. It can be easily appreciated that a fit using a viscoelastic model only (top panel) does not properly describe the IXS data, leading to a poor fit of both the elastic line and the inelastic part of the spectrum (the reduced χ^2 results to be ≈ 2, i.e., more than $10\sigma_{\chi^2}$ larger than its expected value). The inclusion of a second inelastic excitation significantly improves the quality of the fit (reduced $\chi^2 \approx 1$, $\sigma_{\chi^2} \approx 0.1$), as can be seen in the lower panel. For all fitted spectra, the value of χ^2 remained within one standard deviation from the expected value.

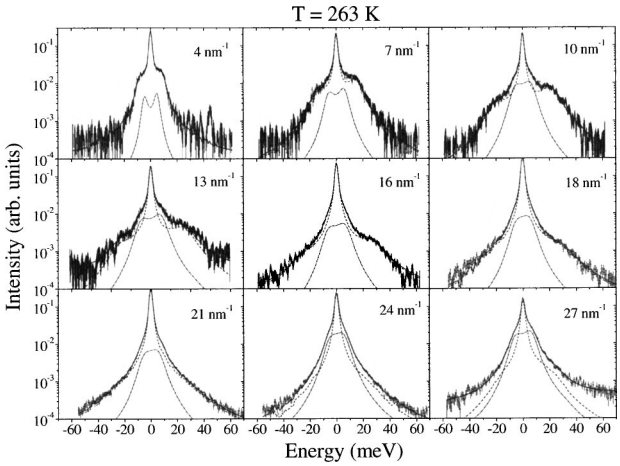

FIG. 2. IXS spectra of water at $T=263$ K and $P=2$ kbar. The figure reports the data (dots) normalized to the total integrated intensity on a logarithmic scale emphasizing the inelastic part of the spectrum. The solid line represents the total fit result as explained in the text, while the other lines visualize the two contributions to the fitting model: the longitudinal and quasielastic one represented by a viscoelastic model (dashed line) and the transverselike secondary peak accounted for by a DHO model function (dash-dotted line).

Figure 2 shows as an example the Q evolution of the IXS data recorded at $T=263$ K and $P=2000$ bar. The two inelastic contributions which clearly appear at $Q=10$ nm^{-1} can also be seen throughout the whole Q range. As can be noticed by the Q evolution of the dashed and dotted lines (longitudinal and transverselike contributions, respectively) the intensity of the low-frequency (transverselike) mode increases with increasing Q.

The shape of the IXS spectra as well as their Q dependence are markedly different at $T=419$ K and $P=95$ bar (see Fig. 3). The elastic line appears broader, and consequently the low-frequency, nondispersing mode is much less visible. As a matter of fact, it can only be identified in the spectra with $Q \leqslant 13$ nm^{-1}, while for larger Q values the increasing width of the elastic line completely governs the spectral shape. The weak feature at about 45 meV in the spectra at $Q=4$ nm^{-1} is the contribution from the high-pressure cell windows and corresponds to the diamond longitudinal acoustic phonon.

To show an example of the temperature evolution of the IXS spectra, and more specifically, of the behavior of the second weakly dispersing feature, the spectra recorded at $Q=10$ (left panel) and 13 nm^{-1} (right panel) are shown in Fig. 4 at the indicated temperatures. At the lowest temperature, the experimental data are shown together with the best fit to

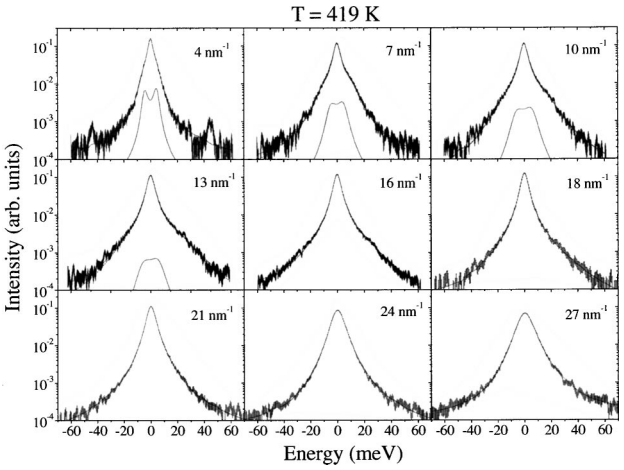

FIG. 3. IXS spectra at $T=419$ K and $P=95$ bar. The figure reports the data (dots) normalized to the total integrated intensity on a logarithmic scale emphasizing the inelastic part of the spectrum. The solid line represents the fit result as explained in the text, while the other lines visualize the two contributions to the fitting model: the longitudinal and quasielastic one represented by a viscoelastic model (dashed line) and the transverselike secondary peak accounted for by a DHO model function (dash-dotted line).

the model function and the two individual components (viscoelastic model and DHO). For the higher temperatures, only the viscoelastic contribution and the total fit are shown for the sake of clarity and in order to emphasize the decreasing importance of the second excitation. We notice a clear trend for both momentum transfers: with increasing temperature the contribution of the second excitation becomes smaller and smaller to the extent that it completely disappears at the highest temperature.

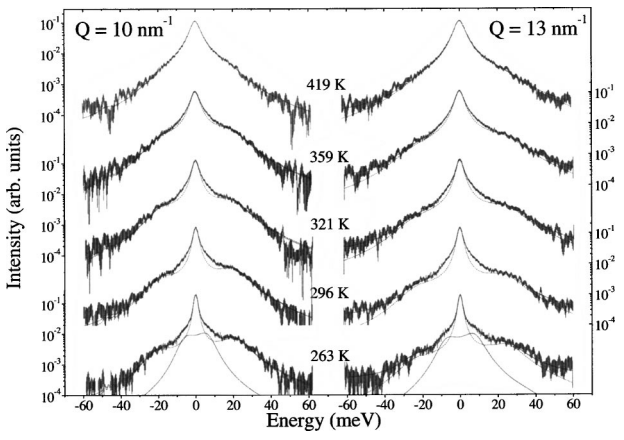

FIG. 4. Temperature evolution of the IXS spectra for $Q=10$ nm^{-1} (left panel) and 13 nm^{-1} (right panel). The figure reports the data (dots) normalized to the total integrated intensity on a logarithmic scale, emphasizing the inelastic part of the spectrum. The solid line represents the fit result as explained in the text, while the other lines visualize the two contributions to the fitting model: the longitudinal and quasielastic one represented by a viscoelastic model (dashed line) and the transverselike secondary peak accounted for by a DHO model function (dash-dotted line).

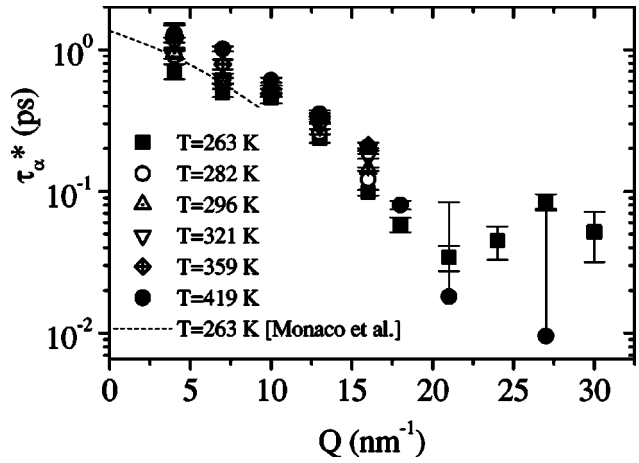

FIG. 5. Q dependence of the (scaled) structural relaxation time $\tau_\alpha^*=\tau_\alpha\eta(T=263\text{ K})/\eta(T)$ (see text). The dashed line reports the fit results of [15] for the Q dependence of the relaxation time at $T=263$ K, valid up to $Q=7$ nm^{-1}.

III. DATA ANALYSIS AND DISCUSSION

A. The longitudinal dynamics

In the present section we present and discuss the results obtained for the longitudinal dynamics which are retrieved from the viscoelastic analysis as described in detail in Sec. II B.

In Fig. 5 we report the Q dependence of the structural relaxation time τ_α at different temperatures T, scaled by the shear viscosity ratio $r(T)=\eta(T=263\text{ K})/\eta(T)$: i.e., $\tau_\alpha^*=r(T)\tau_\alpha(T)$. This scaling has been performed in order to verify whether the structural relaxation time is proportional to the longitudinal viscosity η, a relationship which generally holds in the continuum limit $Q\to 0$. It is evident from the inspection of Fig. 5 that the Q evolution of τ_α at different T is indeed the same, especially in the Q range below 20 nm^{-1}. As implied by the validity of the scaling, the T and the Q dependence of the relaxation time can be factorized:

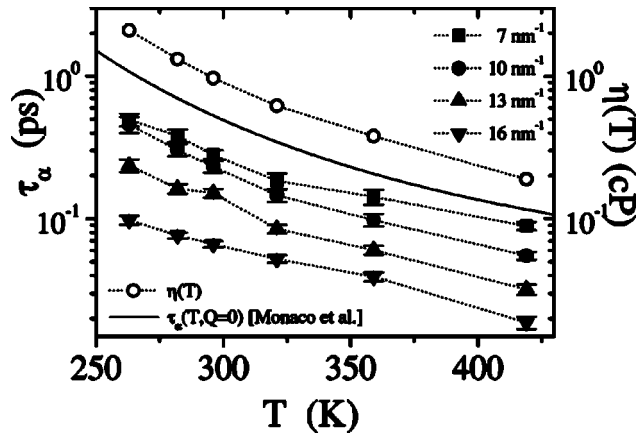

FIG. 6. Temperature evolution of the structural relaxation time (full symbols) at different Q values between 7 and 16 nm^{-1}. The shear viscosity $\eta(T)$ is reported for comparison (open dots), as well as the $Q=0$ extrapolation of the relaxation time [15] (solid line).

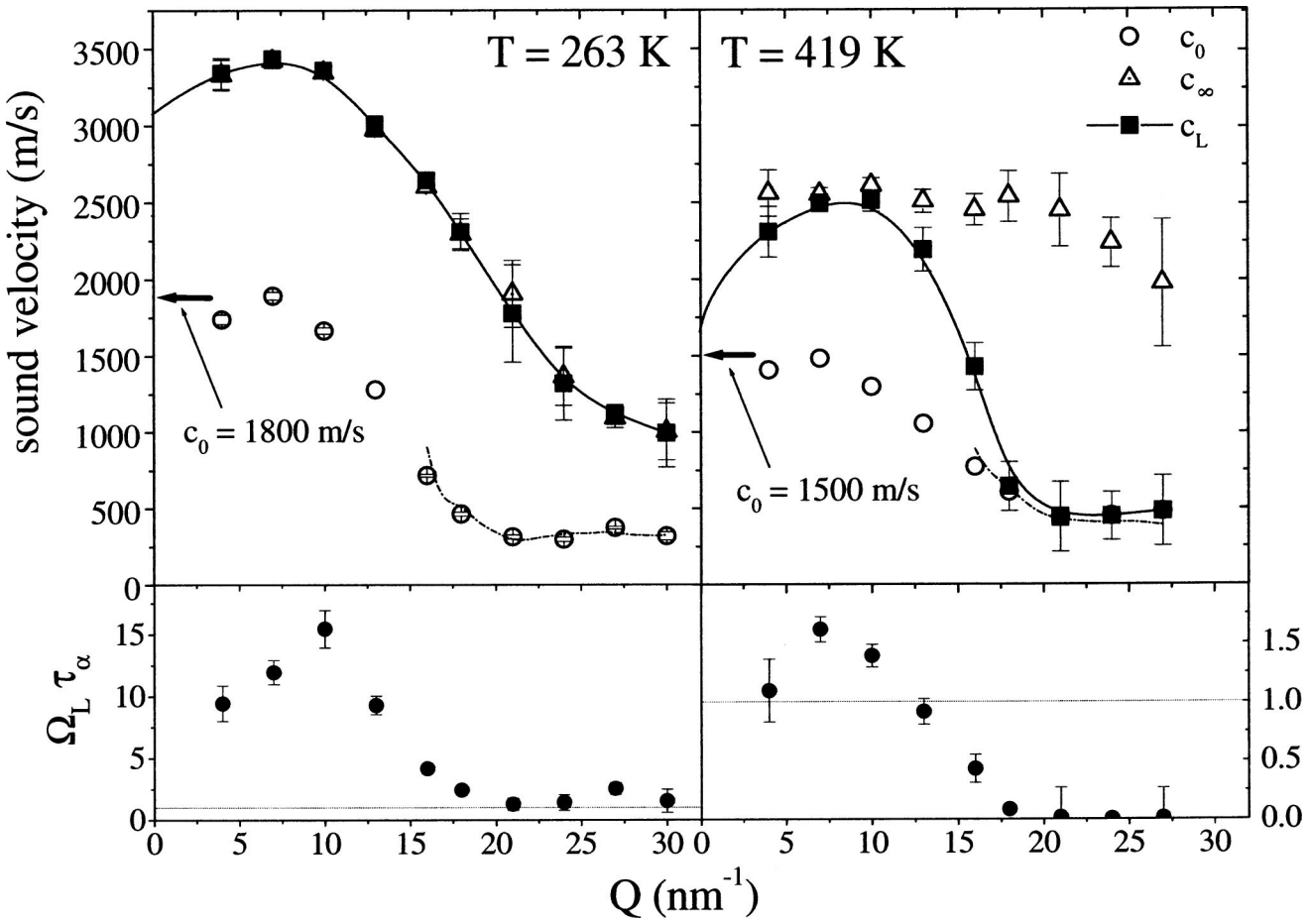

FIG. 7. Sound velocities and the product $\Omega_L\tau_\alpha$—as determined by the fit to the IXS spectra—as a function of Q, and at two different temperatures $T=263$ K (left panels) and 419 K (right panels). The top panels show the Q evolution of the sound velocities c_0 (open dots), c_∞ (open triangles), and c_L (full squares), whereas the bottom panels show the product $\Omega_L\tau_\alpha$, which, when equal to unity, marks the transition from the infinite-frequency sound velocity c_∞ to the zero-frequency sound velocity c_0. The solid line is a guide to the eye. The hydrodynamic ($Q=0$) value of c_0 is indicated by arrows; the Q evolution of $c_0(Q)$, as derived using Eq. (6) and the $S(Q)$ determined by neutron scattering, is indicated by the dash-dotted line in the Q region where neutron data are available. The dotted horizontal line in the lower panels marks the condition $\Omega_L\tau_\alpha=1$.

$\tau_\alpha(Q,T)=\eta(T)f(Q)$, $f(Q)$ being the function that describes the Q evolution of the relaxation time. The dashed line at low Q in Fig. 5 reports the dependence of the relaxation time for $T=263$ K, derived in Ref. [15]; it turns out to be consistent with the present results. Figure 6 shows the temperature dependence of τ_α for different Q values between 7 and 16 nm^{-1}. The evolution of the viscosity (open circles) and the $Q\rightarrow 0$ limit of $\tau_\alpha(Q,T)$ (solid line) as reported in Ref. [15] are also shown. The good overall agreement confirms the reliability of the structural relaxation time determination by the viscoelastic model over the large Q range and in the different thermodynamic conditions investigated here.

The temperature dependence of the zero-frequency sound velocity ($c_0=\omega_0/Q$), the infinite-frequency sound velocity ($c_\infty=\sqrt{(\Delta^2+\omega_0^2)}/Q$), and the apparent sound velocity ($c_L=\Omega_L/Q$) are reported in Fig. 7 for $T=263$ K (left panel) and 419 K (right panel). Here, Ω_L is the maximum of the function $\omega^2 s^{(L)}(Q,\omega)$ calculated using the best fit parameters. The bottom panels of Fig. 7 show the Q dependence of the product $\Omega_L\tau_\alpha$, the parameter that indicates whether the dynamics is viscouslike ($\Omega_L\tau_\alpha<1$) or elasticlike ($\Omega_L\tau_\alpha>1$). For $T=263$ K, $\Omega_L\tau_\alpha$ is always larger than, or close to, 1, the system has a solidlike response, and the sound velocity c_L is close to c_∞, its infinite-frequency value, over the whole explored Q range. In contrast, at $T=419$ K, $\Omega_L\tau_\alpha$ is larger than 1 only over a limited Q range, from 4 to 10 nm^{-1}, and then decreases rapidly below 1 for increasing Q values. Consequently, we observe a transition from the infinite- to the zero-frequency sound regime: it takes place for Q values between 10 and 15 nm^{-1}. This is an experimental observation of the transition $c_\infty\rightarrow c_0$ that takes place for Q values around the Q's where the $S(Q)$ shows its first maximum, as a consequence of the de Gennes narrowing. The Q dependence of the excitation frequency, in fact, shows a decrease with a minimum just in correspondence with the first maximum of the $S(Q)$ as a memory of a "pseudo second Brillouin zone." At the same time the relaxation time decreases toward high Q with respect to the $Q=0$ value with a slight increase at around 27 nm^{-1} again due to de Gennes narrowing (see Fig. 5). Such kind of $c_\infty\rightarrow c_0$ transition, taking place at Q values around the first maximum of the $S(Q)$, has been already ob-

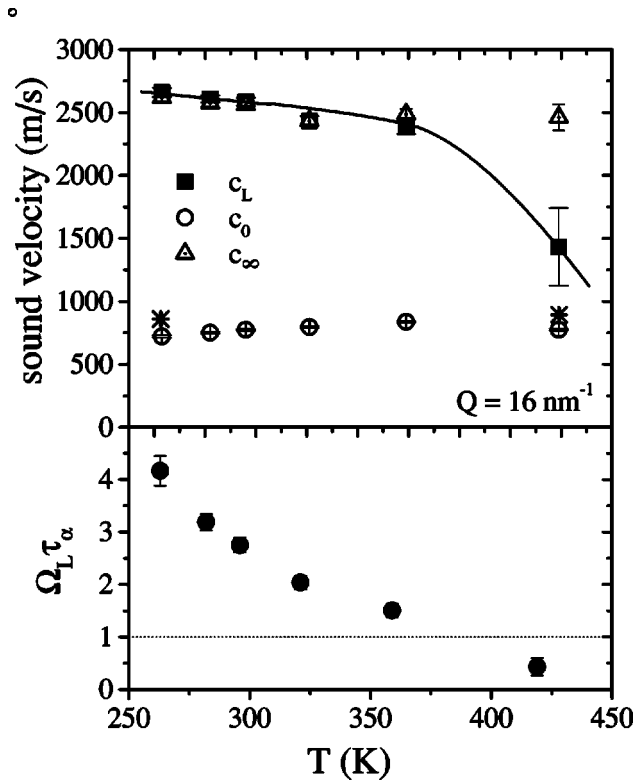

FIG. 8. The temperature dependence of the sound velocities and of the product $\Omega_L\tau_\alpha$ for $Q=16$ nm^{-1}. The data show the same phenomenology as those reported in Fig. 7. Here the product $\Omega_L\tau_\alpha$ is changed by varying the relaxation time scale: as in the previous case we start to observe the transition when we approach $\Omega_L\tau_\alpha \approx 1$. The solid line is a guide to the eye. The stars in the upper panel indicate the $c_0(Q)$ values as derived from Eq. (6) for the thermodynamical points available from the neutron diffraction database [32].

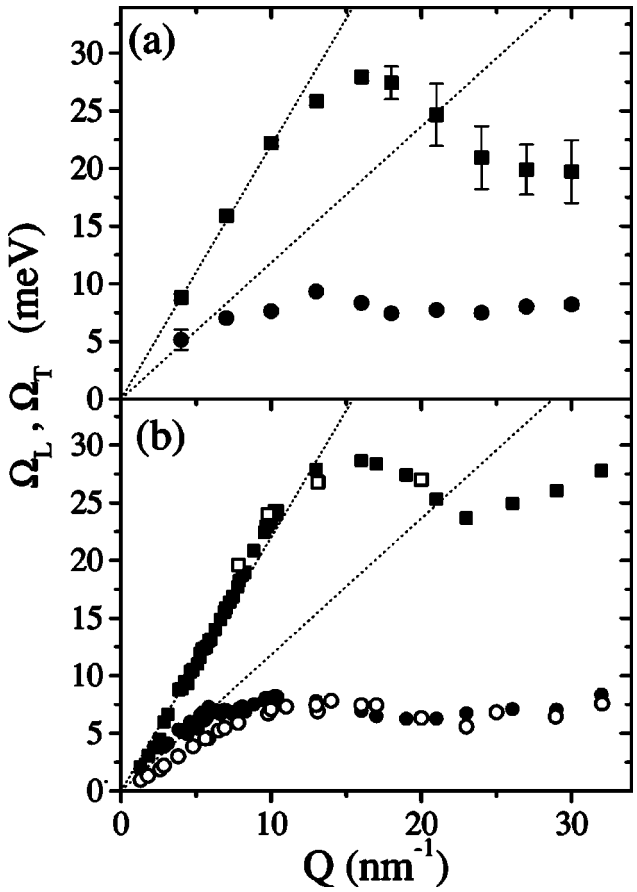

FIG. 9. (a) Longitudinal current peak positions from the fits of IXS data of liquid water at $T=263$ K and $P=2$ kbar. (b) MD simulation results [18] (see text). The dotted lines represent excitations with a linear dispersion in Q, corresponding to sound speeds of 3300 and 1900 m/s, respectively.

served in MD simulations of a Lennard-Jones model glass [31]. Furthermore, we note that our derived values for c_0 is in excellent agreement with independent determinations, both in the limit of $Q\rightarrow 0$ and at high Q values. The values of c_0 in the low-Q limit were obtained from thermodynamic data [21], and are indicated by the arrows in Fig. 7. The zero-frequency sound velocity in the high-Q region (dash-dotted line) has been calculated utilizing the expression for $c_0(Q)$ within the framework of generalized hydrodynamics:

$$c_0 = \sqrt{\frac{k_B T}{MS(Q)}}. \tag{6}$$

Here, we utilized the $S(Q)$ values determined by neutron diffraction measurements [32] at the same thermodynamical conditions (the S_{OO} partial structure factor has been used). The agreement of $c_0(Q)$, calculated using the previous relation and $c_0(Q)$ derived from the fits convincingly demonstrates the solidity of our data analysis procedure.

As expected for a viscoelastic behavior of the excitation, the same $c_0 \leftrightarrows c_\infty$ transition can be observed at fixed Q due to the effect of the temperature on τ_α. Figure 8 shows c_L, c_0, and c_∞ as a function of temperature for $Q=16$ nm^{-1}. At low T the relaxation time is long, $\Omega_L\tau_\alpha \gg 1$, and the apparent sound velocity is close to c_∞. When, on increasing the temperature, the structural relaxation enters the excitation time scale ($\Omega_L\tau_\alpha \approx 1$), the sound velocity c_L recovers its liquidlike value c_0.

B. The second excitation

As already discussed in some detail above, the IXS spectra, especially at low temperature, can only be properly described if one takes into account a second inelastic excitation. This second excitation is described by three parameters (intensity, peak position, and peak width). Figure 9 shows the dispersion (Q dependence) of Ω_T, together with that of Ω_L, at $T=263$ K and $P=2000$ bar, where the second excitation is best appreciated. The upper panel shows the result of the present work. The longitudinal frequency Ω_L (squares) and the "transverse" frequency Ω_T (circles) (both derived from the fit procedure) show the expected behavior: a linear dispersion followed by a bend down and a minimum in the Q region where $S(Q)$ has its maximum for the longitudinal excitation, and a weak Q dependence for the transverse mode. Full symbols in the lower panel correspond to the results of a previous MD simulation [18] for the position of the longi-

tudinal current peaks. These were carried out considering 4000 D_2O molecules enclosed in a cubic box with periodic boundary conditions, and utilizing the SPC/E model [33]. The simulations were performed at a density of 1 g/cm^3 and $T \approx 250$ K. The qualitative agreement between experiment and simulation is remarkable. We note slight differences in the absolute values of the excitation energies: while the maximum of the longitudinal dispersion is slightly lower, the energies for the second excitation are slightly higher in the case of the IXS results. Moreover, a small displacement at higher Q in the position of the first minimum in the IXS data is justified as these are taken at high pressure while the simulations are performed at ambient conditions: as the pressure does not affect very much the value of c_∞ the agreement with the simulation data in the linear region is extremely good. The open symbols, also reported in the lower panel, indicate for some Q values the position of the two peaks found in the transverse current spectrum, a quantity that is not experimentally observable, but that can be determined by MD simulations. The position of these peaks clearly coincides with the corresponding peak measured in the longitudinal current, supporting the presence of a mixing phenomenon [18]. We further note that the energy range over which the weakly dispersing feature is observed corresponds to the TA or TO branch in hexagonal ice as determined by INS [34] and IXS [13].

To further characterize the second excitation we now study its integrated intensity. Specifically, in Fig. 10 we report the "transverse" intensity A_T normalized to the total integrated intensity A_T+A_L as a function of Q for the selected thermodynamic point $T=263$ K and $P=2$ kbar. In the lower panel of Fig. 10, we report the evolution of $\Omega_T\tau_\alpha$. We observe a general increasing trend of the parameter $A_T/(A_T+A_L)$ with increasing Q. It is worth observing that the appearance of a transverselike contribution with an intensity increasing with Q has also been registered in experiments and simulations on glassy systems such as glycerol [35] and silica [27,36,37]. In silica the mixing phenomenon turns out to be particularly enhanced in both MD simulation and experiments indicating that, as in water, the local tetrahedral structure favors the coupling of the L and T dynamics. The intensity increase with Q is expected on the basis of a simple one-excitation picture within the harmonic approximation for the dynamic structure factor, suggesting that, for a nondispersive excitation, $A_T/(A_T+A_L) \approx Q^2$. More importantly, we also observe that, superimposed on the growth of $A_T/(A_T+A_L)$ with Q, there is also a "modulation" in phase with $\Omega_T\tau_\alpha$. When, at $Q \approx 15$ nm^{-1}, $\Omega_T\tau_\alpha$ become less than unity, the intensity of the "transverse" peak decreases.

The presence of a strong correlation between the intensity of the transverse peak and the $\Omega_T\tau_\alpha$ is confirmed by inspecting their temperature evolution reported in Fig. 11 for two selected Q values: $Q=10$ and 13 nm^{-1}. Here, when the time scale of the α relaxation is comparable to the inverse of the frequency of the transverse excitation, the ratio $A_T/(A_T+A_L)$ decreases, and for the highest temperature becomes essentially zero. This behavior—very different from that of the longitudinal collective mode, which is affected by the relaxation only in the sound velocity value—is just the one expected for a transverselike excitation: on recovering a liquidlike regime the system is no longer able to give an elastic response to a shear stress and to sustain propagating transverse waves. In this regime the transverse dynamics assumes a purely relaxational behavior, corresponding to a peak at $\omega=0$ in the current spectrum [22]. For this reason, still lack-

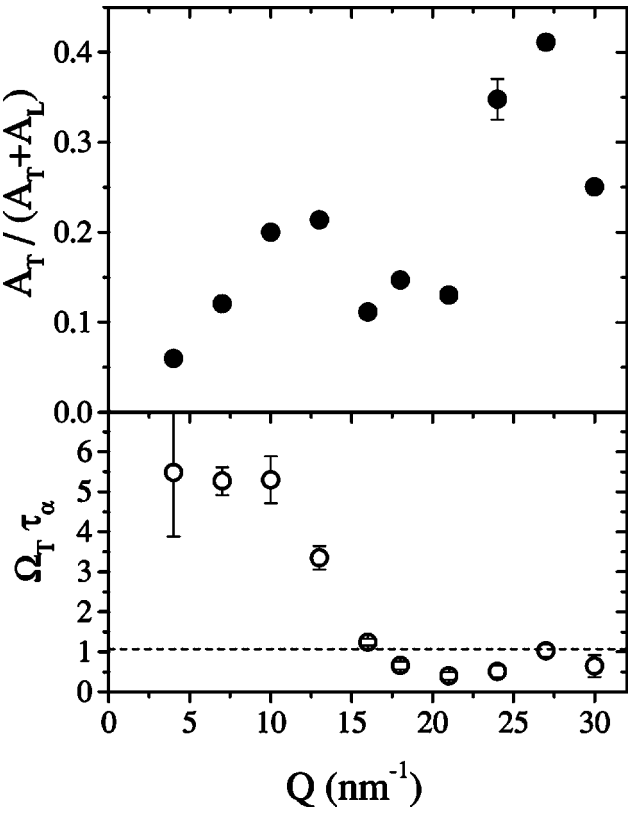

FIG. 10. Q dependence of the transverse to total integrated intensity ratio (upper panel) and the product $\Omega_T\tau_\alpha$ (lower panel) at $T=263$ K. The dashed horizontal line indicates the condition $\Omega_T\tau_\alpha=1$.

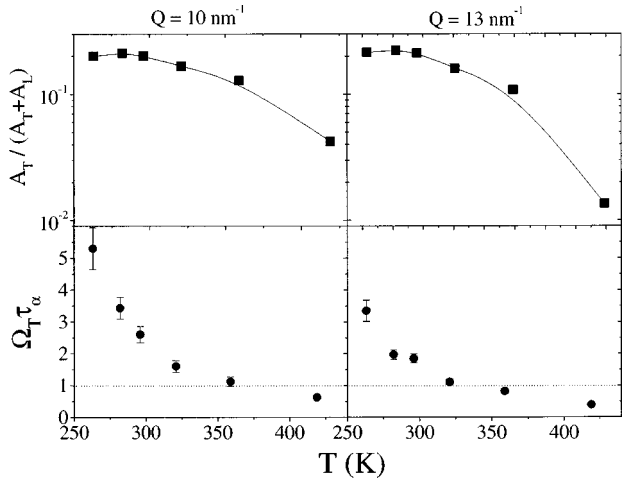

FIG. 11. Top panels: temperature evolution of the transverse to total integrated intensity ratio $A_T/(A_T+A_L)$ at momentum transfers of 10 nm^{-1} (left panel) and 13 nm^{-1} (right panel). The solid lines are guides to the eye. Bottom panels: temperature evolution of $\Omega_T\tau_\alpha$. The dotted horizontal line marks the condition $\Omega_T\tau_\alpha=1$.

ing a formal model for the coupling, the fits at higher temperatures have been performed just fixing the DHO parameters at the lowest T values leaving the intensity A_T free. This procedure allows us to provide the information on the inelastic contribution of the dispersionless mode, leaving the relaxational behavior accounted for by the viscoelastic model. This procedure, as can be seen by bare eye in the spectra at high T, also does not affect at all the statistical significance of the fits when the transverselike contribution, which was mandatory at low T, can be completely neglected.

IV. CONCLUSIONS

In this paper the viscoelastic analysis of the IXS spectra of water, already successfully performed in the low-Q range, has been extended to much larger Q values and in a wide range of thermodynamical conditions.

At the high Q values investigated here the presence of a second excitation in the spectra cannot be neglected anymore and it has been successfully taken into account in the analysis, revealing a behavior in agreement with the viscoelastic expectation for a transverselike excitation. These findings confirm our assignment of a transverse nature to the dispersionless mode of water observed at an energy of ≈ 6 meV.

Furthermore, the large variation of the structural relaxation time (almost a decade) in the investigated thermodynamic range has allowed us to perform an excellent test of the viscoelastic picture. Summarizing, the two main results of the present work are as follows.

(1) The longitudinal-like dynamics can be properly accounted for by a viscoelastic model also in the high-Q range: indeed, in addition to the now well-known transition from c_O to c_∞ that takes place at small Q ($Q \approx 4$ nm^{-1} at ambient conditions), the transition from c_∞ back to c_0, taking place at high Q values, could be observed. This back transition is a consequence of the de Gennes narrowing on the product $\Omega_L \tau_\alpha$, which becomes smaller than 1 at Q values around the Q's of the main peak in the $S(Q)$.

(2) The second dispersionless mode behaves as a transverselike excitation disappearing from the spectra as soon as the structural relaxation process reaches the excitation time scale ($\Omega_T \tau_\alpha = 1$).

Finally, a few words must be devoted to the comparison between the present—viscoelastic—explanation of the high-frequency dynamics of water and the alternative—solid-based—description as discussed in the Introduction. With this purpose we compare in Fig. 12 the temperature behavior of the longitudinal and transverse dynamics for a fixed Q value ($Q = 10$ nm^{-1}). In panel (a) we report the velocities plot as in Fig. 8 (here for a different Q value) while in panel (b) we report the (normalized) intensity of the dispersionless mode at the same Q value. The comparison of the two uppermost panels in Fig. 12 clearly demonstrates that while the apparent sound velocity [c_L, full squares in panel (a)] is still far from c_0 (open dots)—i.e., the system is in the elastic limit over the whole T range—the intensity of the second excitation becomes negligible at high T. Thus we have that, at high T, the system is in the elastic regime, but the second excitation can no longer be appreciated in the spectra. This evidence cannot be framed in the interaction model proposed in Refs. [9,10] which traces the "fast sound" phenomenon back to the presence of and the interaction between two modes. This observation, however, has a clear explanation in the viscoelastic picture as illustrated in panel (c). While the structural relaxation process has already reached the transverselike mode time scales, with $\Omega_T \tau_\alpha < 1$ for $T > 370$ K, thus entering the viscous regime, it is still not affecting the higher-energy longitudinal-like excitation, which still exhib-

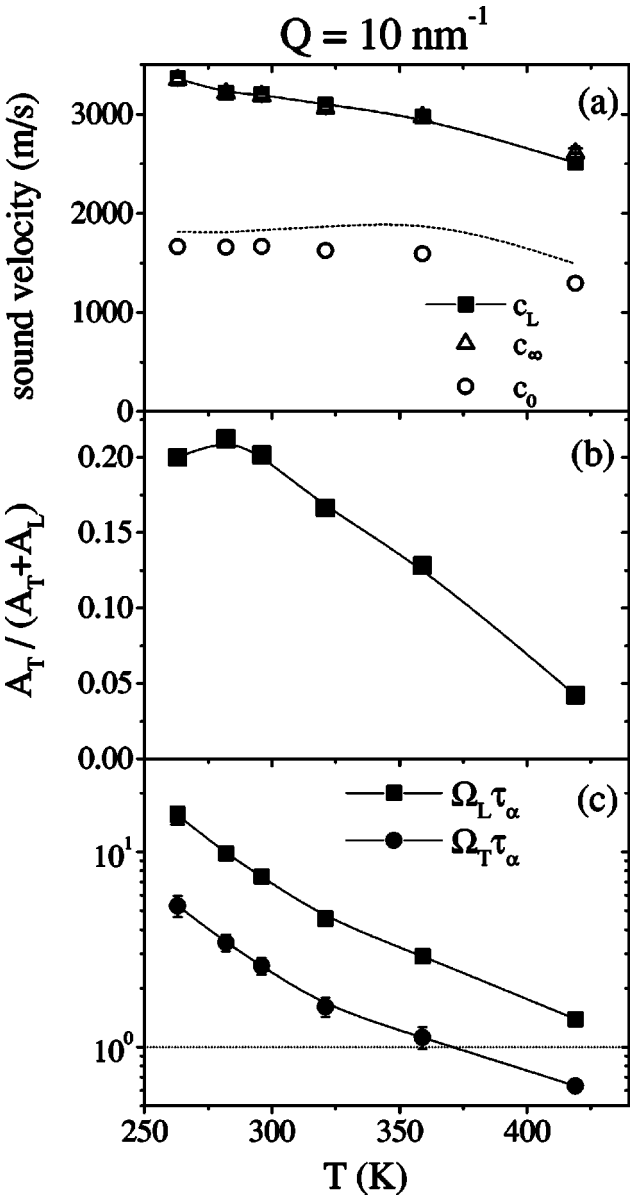

FIG. 12. Comparison of the temperature evolution of the L-like and T-like dynamics for a fixed Q value ($Q = 10$ nm^{-1}). (a) Evolution of the three velocities as in Fig. 8; the dashed line corresponds to the thermodynamic prediction for c_0. (b) Temperature evolution of the transverse to total integrated intensity ratio $A_T/(A_T+A_L)$. (c) Temperature evolution of $\Omega_T \tau_\alpha$ and $\Omega_L \tau_\alpha$; the dotted horizontal line marks the condition $\Omega \tau_\alpha = 1$ clearly showing that the two dynamics are in different regimes at high T. The solid lines are guides to the eye.

its an elastic response ($\Omega_L \tau_\alpha > 1$ up to the highest explored temperature).

The data reported in Fig. 12, together with the outcomes listed in items (1) and (2) before, are the main results of this paper. All these results favor the viscoelastic description of the high-frequency dynamics of water. As a final observation, it must be noted that the two models discussed before are not so different as it appears at a first glance: in both cases it is the interaction of the sound waves with another "mode" which causes both the positive dispersion of the apparent sound velocity and the appearance of a second peak in the dynamic structure factor. In the viscoelastic case the second mode is purely relaxing; in the solidlike approaches the second modes have a propagating component. However, major differences arise in interpreting the physical meaning of the parameters entering in the models. (i) In the solidlike model no information of the structural relaxation time is contained, while τ_α is directly measurable in the viscoelastic model. It is in agreement with independent determinations [14,15], and its values allow us to calculate the viscosity, again in agreement with independent measurements [15]. (ii) Further evidence, again in the same direction, comes from the temperature dependence of the energy of the second mode. In the solidlike framework at increasing temperature the data indicate a decrease of the interaction parameter, corresponding to a decrease of the energy position of the dispersionless mode. This decrease of the energy of the dispersionless mode is not observed; for example, depolarized light scattering measurements [38] do not show any noticeable shift in the position of the peak that corresponds to the density of states of the second excitation. (iii) Finally, let us observe that the viscoelastic-based explanation of the dynamics of the density fluctuations is actually considered the proper approach in many liquids [39] and it has been substantiated by rigorous theories such as the mode coupling theory [40] (a theory that, via MD, has been proved to work properly also in liquid water [41]). In other words, as the dynamic of liquid water shows the same phenomenology as that of many other liquids, why, in water, should one look for a different explanation?

ACKNOWLEDGMENT

We thank M. A. Ricci for pointing out the neutron diffraction database [32].

[1] C. A. Angell, in *Water: A Comprehensive Treatise*, edited by F. Franks (Plenum, New York, 1981), Vol. 7.
[2] P. G. Debenedetti, *Metastable Liquids* (Princeton University Press, Princeton, NJ, 1996).
[3] C. Roenne, L. Thrane, P.-O. Astrand, A. Wallqvist, K. V. Mikkelsen, and S. R. Keiding, J. Chem. Phys. **107**, 5319 (1997).
[4] R. Torre, P. Bartolini, and R. Righini, Nature (London) **428**, 296 (2004)
[5] L. van Hove, Phys. Rev. **95**, 249 (1954).
[6] P. Bosi, F. Dupre, F. Menzinger, F. Sacchetti, and M. C. Spinelli, Lett. Nuovo Cimento Soc. Ital. Fis. **21**, 436 (1978).
[7] J. Teixeira, M.-C. Bellissent-Funel, S. H. Chen, and B. Dorner, Phys. Rev. Lett. **54**, 2681 (1985).
[8] F. J. Bermejo, M. Alvarez, S. M. Bennington, and R. Vallauri, Phys. Rev. E **51**, 2250 (1995).
[9] C. Petrillo, F. Sacchetti, B. Dorner, and J.-B. Suck, Phys. Rev. E **62**, 3611 (2000).
[10] F. Sacchetti, J.-B. Suck, C. Petrillo, and B. Dorner, Phys. Rev. E **69**, 061203 (2004).
[11] F. Sette, G. Ruocco, M. Krisch, U. Bergmann, C. Masciovecchio, V. Mazzacurati, G. Signorelli, and R. Verbeni. Phys. Rev. Lett. **75**, 850 (1995).
[12] G. Ruocco, F. Sette, M. Krisch, U. Bergmann, C. Masciovecchio, V. Mazzacurati, G. Signorelli, and R. Verbeni, Nature (London) **379**, 521 (1996).
[13] F. Sette, G. Ruocco, M. Krisch, C. Masciovecchio, R. Verbeni, and U. Bergmann, Phys. Rev. Lett. **77**, 83 (1996).
[14] A. Cunsolo, G. Ruocco, F. Sette, C. Masciovecchio, A. Mermet, G. Monaco, M. Sampoli, and R. Verbeni, Phys. Rev. Lett. **82**, 775 (1999).
[15] G. Monaco, A. Cunsolo, G. Ruocco, and F. Sette, Phys. Rev. E **60**, 5505 (1999).
[16] G. Ruocco and F. Sette, J. Phys.: Condens. Matter **11**, R259 (1999).
[17] M. Krisch *et al.*, Phys. Rev. Lett. **89**, 125502 (2002).
[18] M. Sampoli, G. Ruocco, and F. Sette, Phys. Rev. Lett. **79**, 1678 (1997).
[19] It is worth pointing out that this is not different from what is proposed in [13] as the optic mode supported by Petrillo *et al.* [9] is the gapless prosecution of the TA mode in an extended Brillouin zone zone description of the phononlike dynamics.
[20] EURISYS Mesures, Lingolsheim, France.
[21] A. Saul and W. Wagner, J. Phys. Chem. Ref. Data **18**, 1537 (1989).
[22] J. P. Boon and S. Yip, *Molecular Hydrodynamics* (Dover, New York, 1991).
[23] U. Balucani and M. Zoppi, *Dynamics of the Liquid State* (McGraw-Hill, New York, 1980).
[24] A. Cunsolo, G. Pratesi, R. Verbeni, D. Colognesi, G. Monaco, C. Masciovecchio, G. Ruocco, and F. Sette, J. Chem. Phys. **114**, 2259 (2001).
[25] T. Scopigno, G. Ruocco, F. Sette, and G. Viliani, Phys. Rev. E **66**, 031205 (2002).
[26] G. Monaco, D. Fioretto, L. Comez, and G. Ruocco, Phys. Rev. E **63**, 061502 (2001).
[27] G. Ruocco and F. Sette, J. Phys.: Condens. Matter **13**, 9141 (2001).
[28] G. Harrison, *The Dynamical Properties of Supercooled Liquids* (Academic, New York, 1976).
[29] C. Masciovecchio, S. C. Santucci, A. Gessini, S. Di Fonzo, G. Ruocco, and F. Sette, Phys. Rev. Lett. **92**, 255507 (2004).
[30] B. Fak and B. Dorner, Institut Laue Langevin (Grenoble, France), Technical Report No. 92FA008S, 1992 (unpublished).

[31] G. Ruocco, F. Sette, R. Di Leonardo, G. Monaco, M. Sampoli, T. Scopigno, and G. Viliani, Phys. Rev. Lett. **84**, 5788 (2000).
[32] http://www.isis.rl.ac.uk/disordered/Database/DBMain.htm
[33] H. J. C. Berendsen, J. P.M. Postma, W. F. Van Gunsteren, and H. J. Hermans, in *Intermolecular Forces*, edited by B. Pulman (Reidel, Dordrecht, 1981), p. 331.
[34] B. Renker, Phys. Lett. **30A**, 493 (1969).
[35] T. Scopigno, E. Pontecorvo, R. Di Leonardo, M. Krisch, G. Monaco, G. Ruocco, B. Ruzicka, and F. Sette, J. Phys.: Condens. Matter **15**, S1269 (2003).
[36] R. Dell'Anna, G. Ruocco, M. Sampoli, and G. Viliani, Phys. Rev. Lett. **80**, 1236 (1998).
[37] B. Ruzicka, T. Scopigno, S. Caponi, A. Fontana, O. Pilla, P. Giura, G. Monaco, E. Pontecorvo, G. Ruocco, and F. Sette, Phys. Rev. B **69**, 100201(R) (2004).
[38] A. P. Sokolov, J. Hurst, and D. Quitmann, Phys. Rev. B **51**, 12865 (1995).
[39] See, for example, Proceedings of the Third Workshop on Non-Equilibrium Phenomena in Supercooled Fluids, Glasses and Amorphous Materials [J. Phys.: Condens. Matter Vol. **15**, S737 (2003)].
[40] W. Goetze and L. Sjogren, Rep. Prog. Phys. **55**, 241 (1992); W. Goetze, J. Phys.: Condens. Matter **11**, A1 (1999); H. Z. Cummins, *ibid.* **11**, A95 (1999).
[41] P. Gallo, F. Sciortino, P. Tartaglia, and S. H. Chen, Phys. Rev. Lett. **76**, 2730 (1996); F. Sciortino, P. Gallo, P. Tartaglia, and S. H. Chen, Phys. Rev. E **54**, 6331 (1996); S. H. Chen, P. Gallo, F. Sciortino, and P. Tartaglia, *ibid.* **56**, 4231 (1996); F. W. Starr, S. Harrington, F. Sciortino, and H. E. Stanley, Phys. Rev. Lett. **82**, 3629 (1999); F. W. Starr, F. Sciortino, and H. E. Stanley, Phys. Rev. E **60**, 6757 (1999); L. Fabbian, A. Latz, R. Schilling, F. Sciortino, P. Tartaglia, and C. Theis, *ibid.* **60**, 5768 (1999).